Vapor–Solid Growth of Few-Layer Graphene Using Radio Frequency Sputtering Deposition and Its Application on Field Emission

Jian-hua Deng,[†] Rui-ting Zheng,[†] Yong Zhao,[‡] and Guo-an Cheng[†,*]

[†]Key Laboratory of Beam Technology and Material Modification of the Ministry of Education, College of Nuclear Science and Technology, Beijing Normal University, Beijing 100875, People's Republic of China and [‡]Department of Physics, Nanchang University, Jiangxi 330031, People's Republic of China

ABSTRACT

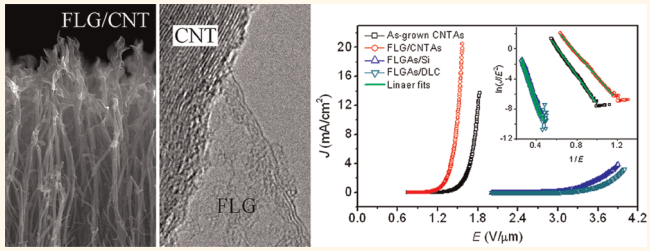

The carbon nanotube (CNT) and graphene hybrid is an attractive candidate for field emission (FE) because of its unique properties, such as high conductivity, large aspect ratio of CNT, and numerous sharp edges of graphene. We report here a vapor–solid growth of few-layer graphene (FLG, less than 10 layers) on CNTs (FLG/CNT) and Si wafers using a radio frequency sputtering deposition system. Based on SEM, TEM, and Raman spectrum analyses, a defect nucleation mechanism of the FLG growth was proposed. The FE measurements indicate that the FLG/CNT hybrids have low turn-on (0.956 V/μm) and threshold fields (1.497 V/μm), large field enhancement factor (~4398), and good stability. Excellent FE properties of the FLG/CNT hybrids make them attractive candidates as high-performance field emitters.

KEYWORDS: few-layer graphene · multiwalled carbon nanotubes · hybrid vapor–solid growth · field emission

Since its discovery,[1] tremendous interest has been stimulated by graphene due to its unique electrical properties, such as its quantum Hall effect at room temperature,[2–4] ambipolar electric field effect,[1] high charge mobility,[5] and transport via relativistic Dirac fermions.[6,7] Graphene has been used to fabricate field effect transistors,[8] gas sensors,[9] photodetectors,[10] resonators,[11] and other devices. Recently, more and more scientists are paying attention to graphene's few-layer counterparts. Few-layer graphene (FLG), named from its nature of 3–10 graphite layers, has been extensively studied due to its similar electrical properties to graphene and because it is easy to fabricate.[12–16]

Up to now, several methods have been used to prepare graphene, such as mechanical exfoliation of highly oriented pyrolytic graphite,[1] chemical exfoliation of graphite on SiO_2/Si,[16,17] epitaxial growth on SiC,[18–20] oxidation and thermal expansion of graphite,[21,22] and chemical vapor deposition (CVD) on metal catalysts.[23–26] However, conventional CVD usually involves a catalyst and carbonaceous gas, which make the graphene grow rapidly and less controllably. Here we report an approach to synthesizing FLG on carbon nanotube arrays (CNTAs), Si wafers, and diamond-like carbon (DLC) films using radio frequency (rf) hydrogen plasma sputtering deposition. FLGs grow extremely slowly without the help of a catalyst and carbonaceous gas. The growth of FLG is discussed based on a defect nucleation and diffusion growth mechanism.

There are few attempts of *in situ* growth of graphene on carbon nanotubes (CNTs). This novel graphene/CNT hybrid material may find potential applications in high-performance field emitters considering a synergistic effect of CNTs (high aspect ratio) and graphene (numerous sharp edges). Here we also report the FE properties of the FLG/CNT hybrids, and this novel material has much better FE performances than the as-grown CNTAs, the FLG arrays grown on Si wafers (FLGAs/Si), and the FLG arrays grown on DLC films (FLGAs/DLC).

RESULTS AND DISCUSSION

Structural Characterization of FLG/CNTAs and FLGAs/Si. In this paper, three types of substrates, CNTAs, Si wafers, and DLC films, were used in the same FLG growth conditions for comparison. A radio frequency (13.56 MHz)

* Address correspondence to gacheng@bnu.edu.cn.

Received for review August 23, 2011 and accepted April 8, 2012.

Published online April 09, 2012
10.1021/nn300900v

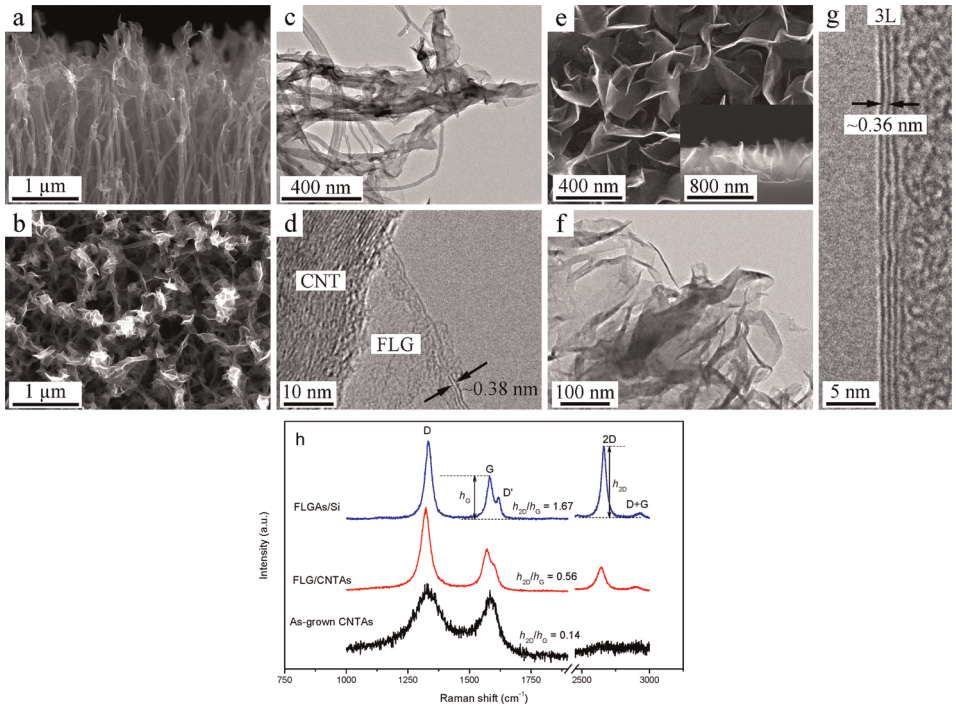

Figure 1. SEM, TEM, and Raman characterizations of FLGs grown on CNTAs (FLG/CNTAs) and Si wafers (FLGAs/Si). (a) SEM side-view image of the FLG/CNTAs. (b) SEM top-view image of the FLG/CNTAs. (c) Low-magnification TEM image of the FLG/CNTAs. (d) High-resolution TEM image of the FLG/CNTAs showing a hybrid structure. (e) SEM top-view and side-view (inset) images of the FLGAs/Si. (f) Typical low-magnification TEM image of the FLGAs/Si. (g) High-resolution TEM image of a curled up FLG edge with ~3 graphite layers (3L). (h) Raman spectra (633 nm laser wavelength) of the as-grown CNTAs, the FLG/CNTAs, and the FLGAs/Si. h_{2D} and h_G are heights of the Raman 2D peak and G peak, respectively. Growth conditions: 300 W, 300 Pa, H_2 (2.5 sccm), 1000 K, 10 h.

sputtering system was employed to synthesize the FLG. High-purity H_2 (99.999%) and a graphite plate (99.5%) were respectively used as the sputtering gas and the sputtering target. The distance between the graphite target and the substrates was about 6 cm. During the FLG growth, the rf power, the substrate temperature, the H_2 gas flow, and the pressure were fixed at 300 W, 1000 K, 2.5 sccm, and 300 Pa, respectively.

The morphology and structure of FLGs grown on nanostructured CNTAs and planar Si wafers were characterized by scanning electron microscope (SEM), transmission electron microscope (TEM), and Raman spectroscopy (633 nm), as shown in Figure 1. It could be observed that sparsely distributed FLGs of 200−300 nm in length and 100−150 nm in width are deposited on the tips of CNTs (Figure 1a−c), which are absent in the as-grown CNTAs; see Supporting Information Figure S1a,b. Due to the densely packed nature of the CNTAs, it is difficult for carbon atoms to go down to the root of CNTs, so the density of FLGs decreases rapidly from the top to the end of CNTs. The FLGs on CNTs are well separated with sharp edges unfolded outside, which weakens field screening during FE and therefore ensures electron tunneling through barriers.[27] Figure 1d is the high-resolution TEM image of a FLG/CNT hybrid, showing that a FLG with 1−3 layers grows firmly against a CNT. The connection between FLG and CNT is hard to observe in TEM when the FLG is thin due to the distortion of FLG, but we did observe similar hybrids with thick FLGs, which present clear atom arrangement at the joints (Supporting Information Figure S2), suggesting that the FLG grows on CNT by sharing carbon atoms rather than being adhered to it. The FLGs grown on Si wafers at the same experimental conditions are 400−500 nm in diameter (inset of Figure 1e), with high density and good separation (Figure 1e). In comparison, the FLGs grown on the CNTs are smaller and sparser than those on the Si wafers. Figure 1f is a low-magnification TEM image of FLGs grown on Si wafers. Intrinsic morphologies such as corrugations and wrinkles are clearly observed in our FLGs.[28] Figure 1g presents a curled up FLG edge with ~3 graphite layers, the full-view image of which is shown in the Supporting Information, Figure S3. We would like to point out that the layer number of most FLGs in our study is less than 10 whether the substrate is a CNT array, a DLC film, or a Si wafer. The interlayer spacing of FLGs, in most cases, is larger than that of the typical bulk graphite (0.34 nm), suggesting a reduction of the van der Waals interaction.

Figure 1h shows Raman spectra of the as-grown CNTAs, the FLG/CNTAs, and the FLGAs/Si. For both types of FLGs, a symmetric single 2D peak at around 2661 cm^{-1} is observed, which stems from the second order of the zone-boundary phonons and is closely related to the layer number of graphene.[29] The height ratio of the 2D peak and G peak, h_{2D}/h_G, has usually being adopted to evaluate the FLG. A larger h_{2D}/h_G ratio is in conformity with graphene of quite few

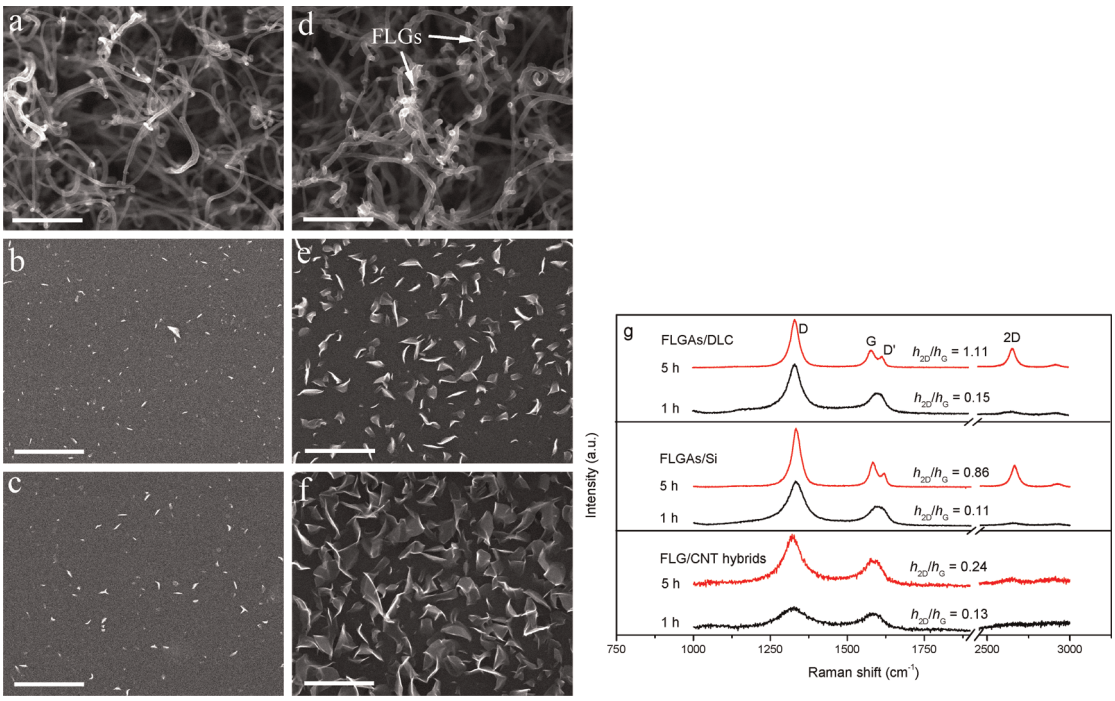

Figure 2. SEM top-view images of 1 h FLG growth on (a) CNTAs, (b) Si wafers, and (c) DLC films. SEM top-view images of 5 h FLG growth on (d) CNTAs, (e) Si wafers, and (f) DLC films. (g) Corresponding Raman spectra of FLGs grown on different substrates within 1 and 5 h, respectively. Other growth conditions are 300 W, 300 Pa, H_2 (2.5 sccm), 1000 K. Scale bar: 500 nm.

layers.[29] The h_{2D}/h_G ratio of the FLGAs/Si is around 1.67, indicating that these FLGs are high-quality superthin graphene. The h_{2D}/h_G ratio of the FLG/CNT hybrids is only about 0.56, mainly due to the small amount of FLGs in the CNTAs, but it is still much larger than the ratio of the as-grown CNTAs (~0.14).

Morphological Evolution of FLG. In order to understand the growth process of FLG, structures of samples with different growth time were characterized by SEM and Raman, as shown in Figure 2. After one hour of plasma processing, it can be observed that the CNTAs (Figure 2a) still look like their primary state (see Supporting Information Figure S1b), but spot-like and needle-like nanostructures appear on the Si wafers (Figure 2b) and DLC films (Figure 2c). The sizes of these nanostructures on DLC films are larger than on Si wafers. After 5 h of growth, small FLGs with the length of 50−100 nm emerge at the tips of CNTs (Figure 2b, marked by arrows). Meanwhile, FLGs that are 100−200 nm in diameter are grown on Si wafers, and FLGs of larger size (250−350 nm in diameter) are observed on DLC films. The morphological evolution of FLGs indicates that the nucleation and growth rate of FLGs changes with the substrate. Figure 2g shows the Raman spectra of FLGs grown on different substrates for 1 and 5 h. The h_{2D}/h_G ratios of the above three samples are quite small (0.11−0.15) after an hour of growth, which is mainly due to the small amount of FLGs. After 5 h, the growth of the FLGs is confirmed by the large h_{2D}/h_G ratio of 0.86 for FLGs grown on Si wafers and 1.11 for FLGs grown on DLC films (the small h_{2D}/h_G ratio of the FLG/CNTAs is due to the small amount of FLGs in the CNTAs).

Nucleation and Growth Mechanism of FLG. Comparing the above three types of substrates, CNTAs with intrinsic defects (see Raman spectrum shown in Figure 1j), Si wafers with perfect surfaces, and DLC films with defective surfaces,[30] we conjecture that the FLG nucleation is defect guided. Figure 3a−g are the schematic diagrams of the defect nucleation and growth mechanism of FLG. For CNTAs (Figure 3a,b), sputtering and hydrogen etching defects and intrinsic growing defects are believed to be the initial positions for FLG growth. On flawless Si wafers (Figure 3c−e), the FLG nucleation starts with a deposition of a thin defective carbon layer that can be detected by the Raman spectrum, in which a carbon-related D peak and G peak[29] are observed after an hour of FLG growth (Figure 2g). Then, the point defects or small-scale defects in this defective carbon layer grow by absorbing activated carbon atoms, for example, by forming large-scale linear defects. For FLG grown on DLC films (Figure 3f,g), the carbon layer growth is accelerated for the abundant defects in DLC. So we conjecture that, for FLGs grown on planar substrates, the relatively slower growth of FLGs on Si wafers than on DLC films is due to the FLG nucleation on the former being postponed. While for FLGs grown on CNTs the nanostructured morphology of CNTs greatly hinders the defect growth, especially in the hydrogen etching ambient, small-scale defects are more likely to be etched away.

According to previous investigations on vertically aligned carbon nanosheets (CNSs),[31−34] sputtered carbon atoms arrive at the CNS and serve as activated

carbon atoms. These activated carbon atoms diffuse on the surface of the CNS and form covalent bonds at the edge before they are re-evaporated. A long enough surface diffusion length of the carbon atom (λ_d, the average distance that a carbon atom can migrate along a flawless graphene surface before being re-evaporated) is essential for the growth of thin CNSs.[31,34] The λ_d in our growth conditions (1000 K) is about 3.2 μm,[31−33] far larger than the diameter of FLGs (less than 500 nm), which means that the activated carbon atoms can migrate to the edges of FLGs and form covalent bonds before being re-evaporated; that is, the FLGs grow in a two-dimensional (2D) way. However, the situation where a carbon atom diffuses on a flawless graphene (Figure 3h) does not exist. There are many carbon atoms that diffuse on the FLG surface at the same time and atomic collisions occur frequently (Figure 3i, labeled by A). Atom−atom collision greatly increases the actual surface diffusion length (λ_{ad}) on the FLG surface. This prolonged diffusion makes the activated carbon atoms more likely to be captured by defects which already exist on the FLG surface (Figure 3i, labeled by B), resulting in the increase of the FLG thickness. We should emphasize that the above discussions about carbon atom diffusion is more a conjecture based on SEM and Raman rather than *in situ* observations; we still cannot figure out the exact diffusion process, which needs to be further understood.

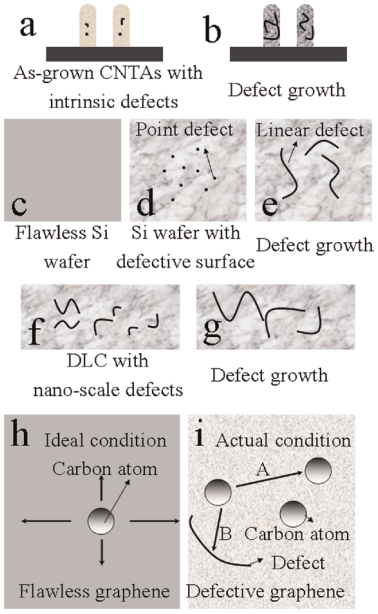

Figure 3. FLG nucleation and atom diffusion. Schematics of (a) as-grown CNTAs with intrinsic defects, (b) defect growth on CNTs, (c) Si wafer with flawless surface, (d) point defects formed on the Si wafer, (e) defect grows on the Si wafer, (f) as-grown DLC film with a great amount of nanoscale defects, and (g) defect growth on the DLC film. Schematics of activated carbon atom diffusion on graphene in (h) ideal conditions and (i) actual conditions; A and B in (i) correspond to atom−atom collision and atom−defect interaction, respectively.

It is hard to measure the exact carbon concentration (C_c) in the sputtering system; alternatively, we can measure the deposition rate of carbon using a MDC-360 oscillation quartz crystal film thickness monitor (MAXTEK, Inc.). The deposition rate of the carbon film is just 7.9 nm/h at room temperature (the thickness monitor can work only at room temperature), which is quite small. The actual deposition rate should be even smaller considering the higher re-evaporation rate of carbon atoms at high temperatures (~1000 K). This small deposition rate means an extremely low C_c in the sputtering chamber and is beneficial to the growth of superthin FLGs according to our above discussions.

Application to Field Emission. The FE properties of FLG hybrids synthesized in the same growth conditions were measured using a diode setup at room temperature (see Methods). Figure 4a plots the emission current density (J) of the as-grown CNTAs, the FLG/CNTAs, the FLGAs/Si, and the FLGAs/DLC (the SEM top view image of FLGAs/DLC is shown in the Supporting Information Figure S4) as a function of the applied field (E), *i.e.*, $J-E$ curves. It is found that the turn-on electric field (E_{on}, 0.956 V/μm at 10 μA/cm^2) and threshold field (E_{th}, 1.497 V/μm at 10 mA/cm^2) of the FLG/CNTAs are

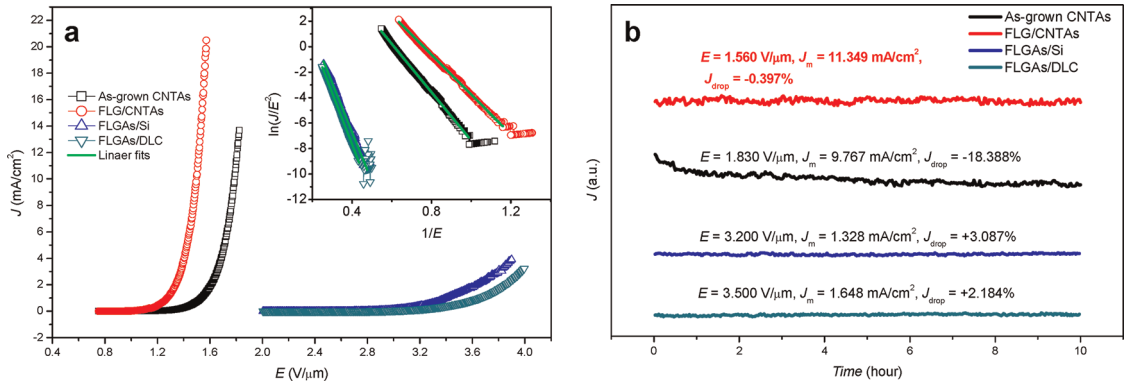

Figure 4. Field emission properties of the as-grown CNTAs, the FLG/CNTAs, the FLGAs/Si, and the FLGAs/DLC. (a) Plots of emission current density (J) as a function of applied filed (E), and the inset is the corresponding $F-N$ plots given in terms of $\ln(J/E^2)$ and $1/E$. (b) Stability of the products displayed in terms of J *versus* time. E: applied field in stability test, J_m: mean emission current density, J_{drop}: emission current degradation, "−" for current degradation and "+" for current increase.

TABLE 1. Field Emission Results of the As-Grown CNTAs, the FLG/CNTAs, the FLGAs/Si, and the FLGAs/DLC

sample	turn-on electric field (V/μm)	threshold field (V/μm)	work function (eV)	field enhancement factor
as-grown CNTAs	1.150	1.787	4.89	3892
FLG/CNTAs	0.956	1.497	4.67	4398
FLGAs/Si	2.525		4.64	1761
FLGAs/DLC	2.690		4.63	1691

significantly lower than those of the as-grown CNTAs (E_{on}, 1.150 V/μm; E_{th}, 1.787 V/μm), the FLGAs/Si (E_{on}, 2.525 V/μm), and the FLGAs/DLC (E_{on}, 2.690 V/μm). The results are listed in Table 1. It is worth noticing that the E_{on} of the FLG/CNTAs is lower than some other low-dimensional materials, such as single-layer graphene films,[35] single-crystalline boron nanowire arrays,[36] and single-crystalline Sb_2Se_3 nanowires.[37] Replotting of the data as $\ln(J/E^2)$ *versus* $1/E$, as shown in the inset of Figure 4a, indicates *F*−*N*-type FE behavior.[38] The work function (Φ) of the emitters was measured using a photoelectron spectrometer. The work functions of the FLG/CNTAs, the FLGAs/Si, and the FLGAs/DLC (4.67, 4.64, and 4.63 eV, respectively) are smaller than that of the as-grown CNTAs (4.89 eV), which may be due to the ascended Fermi level induced by the increased state density of defects during the long-time H plasma processing.[39] With the Φ and the constant *F*−*N* slope in the low-current region, as shown in Table 1, the geometric field enhancement factor (β) of the FLG/CNT hybrids is determined to be ∼4398, which is larger than those of the as-grown CNTAs (∼3892), the FLGAs/Si (∼1761), and the FLGAs/DLC (∼1691). β is closely related to the morphologies of emitters; larger β means larger local electric fields (E_{loc}, $E_{loc} = \beta E_{appl}$, E_{appl} is the electric field applied between the anode and the emitters) at emitter tips and is beneficial to the electron emission. The excellent FE properties of the FLG/CNTAs should be attributed to the increase of effective emission sites, the large aspect ratio of the CNT, and the decrease in work function. The β of FLG/CNTAs is far larger than that of the FLG arrays grown on planar substrates, suggesting that the CNT here plays a role more than a substrate but can improve the FE of the FLGs, also. Furthermore, we consider that the FE properties of FLGAs/Si being better than those of FLGAs/DLC can be ascribed to the insulating nature of the DLC films, which restricts electron transfer from the substrate to the FLG emitters.

The stability of FE devices is quite important in applications. We tested the FE stability behavior of the FLG/CNTAs and the as-grown CNTAs at around 10 mA/cm^2 for 10 h. The largest emission current densities of FLGAs/Si and FLGAs/DLC are far less than 10 mA/cm^2, so we tested their stability behavior at around 1−2 mA/cm^2 for 10 h. The results are shown in Figure 4b. We employ J_{drop} (J degradation during the testing time, calculated by $(J_{first} - J_{last})/J_m$; J_{first}, J_{last}, and J_m, are the first, the last, and the mean emission current density, respectively) to evaluate the stability behavior of these nanoarrays. The FLG/CNTAs (J_{drop}, −0.397%), the FLGAs/Si (J_{drop}, +3.087%), and the FLGAs/DLC (J_{drop}, +2.184%) show better FE stability than the as-grown CNTAs (J_{drop}, −18.388%, "−" for current degradation and "+" for current increase). The excellent FE stability of FLG/CNTAs is better than or comparable to some validated good field emitters reported previously, such as the camphor-grown CNTAs, the J of which drops ∼5% in one week at an initial J of 1 mA/cm^2,[40] and the thermal oxidation processed CNTAs, showing a current degradation of ∼10% in 12 h with a high initial J of 31.6 mA/cm^2.[41] For CNTAs, some protruded CNTs will suffer from an excessive electron emission because of less field-screening,[27] and these CNTs are more likely to be burned off by Joule heat during FE.[42,43] While for 2D planar emitters like FLG, this Joule heating induced emission site decrease can be greatly weakened due to the uniform current distribution on its homogeneous surface. Except for the advantages already mentioned, it should be emphasized that the low applied field at ∼10 mA/cm^2 of the FLG/CNTAs (1.560 V/μm), which is 1.830 V/μm for the as-grown CNTAs, is favorable in practical applications.

CONCLUSIONS

We have demonstrated a simple, controllable, uncatalyzed, and vapor−solid approach to fabricating FLGs (less than 10 layers) on both CNTAs and planar substrates (Si wafers and DLC films) by an rf H plasma sputtering deposition system. On the basis of the SEM, TEM, and Raman characterizations, a defect nucleation mechanism is proposed for the growth of FLG. We also studied the FE properties of the FLG/CNTAs, the FLGAs/Si, and the FLGAs/DLC in comparison with that of the as-grown CNTAs. The FLG/CNTAs show excellent FE properties, with E_{on} = 0.956 V/μm, E_{th} = 1.497 V/μm, a large field enhancement factor of ∼4398, and 0.397% current degradation of around 10 mA/cm^2 in 10 h, which are much better than those of the as-grown CNTAs, the FLGAs/Si, and the FLGAs/DLC. We attribute the excellent FE properties of FLG/CNTAs to the increased effective emission sites from the sharp FLG edges and the decrease of work function. FLG/CNTAs are promising candidates for high-performance field electron emitters.

METHODS

CNT Fabrication. CNTAs were grown by thermal CVD (C_2H_2 as the carbon feedstock) on single-crystal n-Si (100) wafers. First, a 5-nm-thick iron film was deposited on the Si wafers as a catalyst using magnetron sputtering. Then the catalyst was annealed at 580 °C for 1 h under 400 sccm H_2 in a tubular

furnace. Before the growth, the catalyst was etched in 150 sccm NH_3 for 10 min at 750 °C. The growth was then carried out at 750 °C for 30 min under a gas mixture of 600 sccm H_2 and 87 sccm C_2H_2. Then the sample was rapidly cooled to room temperature in H_2 ambient (600 sccm).

DLC Preparation. The DLC films were fabricated via a metal vapor vacuum arc ion source deposition system on single-crystal n-Si (100) wafers at room temperature. The Si wafers were fixated on a rolling stainless specimen holder that was placed in a chamber with a base pressure of 5×10^{-4} Pa. Then the Si wafers were exposed to carbon plasma, which was energized by arc discharge, and a negative bias of ~150 V was applied on the Si wafers. The deposition time was 40 min, during which an approximately 100-nm-thick DLC film was deposited.

FLG Growth. A capacitively coupled rf (13.56 MHz) sputtering system was employed to synthesize FLG. As-grown CNTAs, single crystal n-Si (100) wafers, and Si wafers with ~100-nm-thick DLC films were adopted as the substrates. H_2 was used as the sputtering gas, and the sputtering target is a high-purity graphite plate (99.5%). The deposition was carried out in a chamber that was prepumped to 8.0×10^{-4} Pa. Then the samples were heated by our own designed heater under 2.5 sccm H_2 at 300 Pa. The distance between the graphite target and the substrates was ~6 cm. During the FLG growth, the rf power, the substrate temperature, the H_2 gas flow, and the pressure were 300 W, 1000 K, 2.5 sccm, and 300 Pa, respectively. For morphology observation, the growth time was about 1, 5, and 10 h, respectively.

Field Emission Measurements. A diode setup was placed in a vacuum chamber with the prepared sample (area: 2−4 mm^2) as the cathode and a stainless steel plate as the anode. The distance between the cathode and the anode was 1 mm. The base pressure of the vacuum chamber was $\sim 1 \times 10^{-7}$ Pa, and the temperature was ~288 K (cooled by water). The emission current and the applied voltage were recorded automatically by a computer, and the increasing rate of the applied voltage was 500 V/min.

Characterization. A field emission scanning electron microscope (Hitachi S-4800, 10 kV), a high-resolution transmission electron microscope (JEM-2010, JEOL, 200 kV), and a Raman (LobRAM ARAMIS) with an excitation of 633 nm were employed to characterize the products. A photoelectron spectrometer (AC-2 RIKEM KEIKI, spot area: 4×4 mm^2) was adopted to measure their work functions at room temperature and at ambient pressure.

Conflict of Interest: The authors declare no competing financial interest.

Acknowledgment. This work was supported by the National Basic Research Program of China (No. 2010CB832905), by the Key Scientific and Technological Project of the Ministry of Education of China (No. 108124), and partially by the National Natural Science Foundation of China (No. 11005059).

Supporting Information Available: SEM images of the as-grown CNTAs, HRTEM image of a thick FLG/CNT hybrid, full-view HRTEM image of a FLG, and SEM image of FLG arrays grown on DLC films. These materials are available free of charge *via* the Internet at http://pubs.acs.org.

REFERENCES AND NOTES

1. Novoselov, K. S.; Geim, A. K.; Morozov, S. V.; Jiang, D.; Zhang, Y.; Dubonos, S. V.; Grigorieva, I. V.; Firsov, A. A. Electric Field Effect in Atomically Thin Carbon Films. *Science* **2004**, *306*, 666–669.
2. Novoselov, K. S.; Jiang, Z.; Zhang, Y.; Morozov, S. V.; Stormer, H. L.; Zeitler, U.; Maan, J. C.; Boebinger, G. S.; Kim, P.; Geim, A. K. Room-Temperature Quantum Hall Effect in Graphene. *Science* **2007**, *315*, 1379.
3. Zhang, Y.; Tan, Y. W.; Stormer, H. L.; Kim, P. Experimental Observation of Quantum Hall Effect and Berry's Phase in Graphene. *Nature* **2005**, *438*, 201–204.
4. Nonoselov, K. S.; McCann, E.; Morozov, S. V.; Fal'ko, V. I.; Katsnelson, M. I.; Zeitler, U.; Jiang, D.; Schedin, F.; Geim, A. K. Unconventional Quantum Hall Effect and Berry's Phase of 2π in Bilayer Graphene. *Nat. Phys.* **2006**, *2*, 177–180.
5. Geim, A. K.; Novoselov, K. S. The Rise of Graphene. *Nat. Mater.* **2007**, *6*, 183–191.
6. Zhou, S. Y.; Gweon, G. H.; Graf, J.; Fedorov, A. V.; Spataru, C. D.; Diehl, R. D.; Kopelevich, Y.; Lee, D. H.; Louie, S. G.; Lanzara, A. First Direct Observation of Dirac Fermions in Graphite. *Nat. Phys.* **2006**, *2*, 595–599.
7. Novoselov, K. S.; Geim, A. K.; Morozov, S. V.; Jiang, D.; Katsnelson, M. I.; Grigorieva, I. V.; Dubonos, S. V.; Firsov, A. A. Two-Dimensional Gas of Massless Dirac Fermions in Graphene. *Nature* **2005**, *438*, 197–200.
8. Lin, Y. M.; Dimitrakopoulos, C.; Jenkins, K. A.; Farmer, D. B.; Chiu, H. Y.; Grill, A.; Avouris, P. 100-Ghz Transistors from Wafer-Scale Epitaxial Graphene. *Science* **2010**, *327*, 662.
9. Schedin, F.; Geim, A. K.; Morozov, S. V.; Hill, E. W.; Blake, P.; Katsnelson, M. I.; Novoselov, K. S. Detection of Individual Gas Molecules Adsorbed on Graphene. *Nat. Mater.* **2007**, *6*, 652–655.
10. Xia, F. N.; Mueller, T.; Lin, Y. M.; Garcia, A. V.; Avouris, P. Ultrafast Graphene Photodetector. *Nat. Nanotechnol.* **2009**, *4*, 839–843.
11. Bunch, J. S.; van der Zande, A. M.; Verbridge, S. S.; Frank, I. W.; Tanenbaum, D. M.; Parpia, J. M.; Craighead, H. G.; McEuen, P. L. Electromechanical Resonators from Graphene Sheets. *Science* **2007**, *315*, 490–493.
12. Jung, N.; Kim, N.; Jockusch, S.; Turro, N. J.; Kim, P.; Brus, L. Charge Transfer Chemical Doping of Few Layer Graphenes: Charge Distribution and Band Gap Formation. *Nano Lett.* **2009**, *9*, 4133–4137.
13. Luo, Z. T.; Somers, L. A.; Dan, Y. P.; Ly, T.; Kybert, N. J.; Mele, E. J. Charlie Johnson, A. T. Size-Selective Nanoparticle Growth on Few-Layer Graphene Films. *Nano Lett.* **2010**, *10*, 777–781.
14. Zhang, H. X.; Feng, P. X. Fabrication and Characterization of Few-Layer Graphene. *Carbon* **2010**, *48*, 359–364.
15. Lui, C. H.; Li, Z. Q.; Chen, Z. Y.; Klimov, P. V.; Brus, L. E.; Heinz, T. F. Imaging Stacking Order in Few-Layer Graphene. *Nano Lett.* **2011**, *11*, 164–169.
16. Dimiev, A.; Kosynkin, D. V.; Sinitskii, A.; Slesarev, A.; Sun, Z. Z.; Tour, J. M. Layer-by-Layer Removal of Graphene for Device Patterning. *Science* **2011**, *331*, 1168–1172.
17. Gilje, S.; Han, S.; Wang, M. S.; Wang, K. L.; Kaner, R. B. A Chemical Route to Graphene for Device Applications. *Nano Lett.* **2007**, *7*, 3394–3398.
18. Berger, C.; Song, Z. M.; Li, X. B.; Wu, X. S.; Brown, N.; Naud, C.; Mayou, D.; Li, T. B.; Hass, J.; Marchenkov, A. N.; Conrad, E. H.; First, P. N.; de Heer, W. A. Electronic Confinement and Coherence in Patterned Epitaxial Graphene. *Science* **2006**, *312*, 1191–1196.
19. Berger, C.; Song, Z. M.; Li, T. B.; Li, X. B.; Ogbazghi, A. Y.; Feng, R.; Dai, Z. T.; Marchenkov, A. N.; Conrad, E. H.; First, P. N.; de Heer, W. A. Ultrathin Epitaxial Graphite: 2D Electron Gas Properties and a Route toward Graphene-Based Nanoelectronics. *J. Phys. Chem. B* **2004**, *108*, 19912–19916.
20. Yakes, M. K.; Gunlycke, D.; Tedesco, J. L.; Campbell, P. M.; Myers-Ward, R. L.; Eddy, C. R., Jr.; Gaskill, D. K.; Sheehan, P. E.; Laracuente, A. R. Conductance Anisotropy in Epitaxial Graphene Sheets Generated by Substrate Interactions. *Nano Lett.* **2010**, *10*, 1559–1562.
21. McAllister, M. J.; Li, J. -L.; Adamson, D. H.; Schniepp, H. C.; Abdala, A. A.; Liu, J.; Herrera-Alonso, M.; Milius, D. L.; Car, R.; Prud'homme, R. K.; Aksay, I. A. Single Sheet Functionalized Graphene by Oxidation and Thermal Expansion of Graphite. *Chem. Mater.* **2007**, *19*, 4396–4404.
22. Wei, Z. Q.; Barlow, D. E.; Sheehan, P. E. The Assembly of Single-Layer Graphene Oxide and Graphene Using Molecular Templates. *Nano Lett.* **2008**, *8*, 3141–3145.
23. Li, W.; Tan, C.; Lowe, M. A.; Abruna, H. D.; Ralph, D. C. Electrochemistry of Individual Monolayer Graphene Sheets. *ACS Nano* **2011**, *5*, 2264–2270.
24. Avsar, A.; Yang, T. Y.; Bae, S.; Balakrishnan, J.; Volmer, F.; Jaiswal, M.; Yi, Z.; Ali, S. R.; Güntherodt, G.; Hong, B. H.;

Beschoten, B.; Özyilmaz, B. Toward Wafer Scale Fabrication of Graphene Based Spin Valve Devices. *Nano Lett.* **2011**, *11*, 2363–2368.
25. Kim, K. S.; Zhao, Y.; Jang, H.; Lee, S. Y.; Kim, J. M.; Kim, K. S.; Ahn, J. H.; Kim, P.; Choi, J. Y.; Hong, B. H. Large-Scale Pattern Growth of Graphene Films for Stretchable Transparent Electrodes. *Nature* **2009**, *457*, 706–710.
26. Kim, U. J.; Lee, I. H.; Bae, J. J.; Lee, S.; Han, G. H.; Chae, S. J.; Günes, F.; Choi, J. H.; Baik, C. W.; Kim, S. I.; Kim, J. M.; Lee, Y. H. Graphene/Carbon Nanotube Hybrid-Based Transparent 2D Optical Array. *Adv. Mater.* **2011**, *23*, 3809–3814.
27. Suh, J. S.; Jeong, K. S.; Lee, J. S.; Han, I. Study of the Field-Screening Effect of Highly Ordered Carbon Nanotube Arrays. *Appl. Phys. Lett.* **2002**, *80*, 2392–2394.
28. Ferrari, A. C.; Meyer, J. C.; Scardaci, V.; Casiraghi, C.; Lazzeri, M.; Mauri, F.; Piscanec, S.; Jiang, D.; Novoselov, K. S.; Roth, S.; Geim, A. K. Raman Spectrum of Graphene and Graphene Layers. *Phys. Rev. Lett.* **2006**, *97*, 187401.
29. Meyer, J. C.; Geim, A. K.; Katsnelson, M. I.; Novoselov, K. S.; Booth, T. J.; Roth, S. The Structure of Suspended Graphene Sheets. *Nature* **2007**, *446*, 60–63.
30. Benedikt, J.; Woen, R. V.; van Mensfoort, S. L. M.; Perina, V.; Hong, J.; van de Sanden, M. C. M. Plasma Chemistry during the Deposition of a-C:H Films and Its Influence on Film Properties. *Diamond Relat. Mater.* **2003**, *12*, 90–97.
31. Lewis, B.; Anderson, J. C. *Nucleation and Growth of Thin Films*; Academic: London, 1979; p 51.
32. Lee, Y. H.; Kim, S. G.; Tománek, D. Catalytic Growth of Single-Wall Carbon Nanotubes: An Ab Initio Study. *Phys. Rev. Lett.* **1997**, *78*, 2393–2396.
33. Louchev, O. A.; Sato, Y.; Kanda, H. Growth Mechanism of Carbon Nanotube Forests by Chemical Vapor Deposition. *Appl. Phys. Lett.* **2002**, *80*, 2752–2754.
34. Zhu, M. Y.; Wang, J. J.; Holloway, B. C.; Outlaw, R. A.; Zhao, X.; Hou, K.; Shutthananhdan, V.; Manos, D. M. A Mechanism for Carbon Nanosheet Formation. *Carbon* **2007**, *45*, 2229–2234.
35. Wu, Z. S.; Pei, S. F.; Ren, W. C.; Tang, D. M.; Gao, L. B.; Liu, B. L.; Li, F.; Liu, C.; Cheng, H. M. Field Emission of Single-Layer Graphene Films Prepared by Electrophoretic Deposition. *Adv. Mater.* **2009**, *21*, 1756–1760.
36. Liu, F.; Tian, J. F.; Bao, L. H.; Yang, T. Z.; Shen, C. M.; Lai, X. Y.; Xiao, Z. M.; Xie, W. G.; Deng, S. Z.; Chen, J.; She, J. C.; Xu, N. S.; Gao, H. J. Fabrication of Vertically Aligned Single-Crystalline Boron Nanowire Arrays and Investigation of Their Field-Emission Behavior. *Adv. Mater.* **2008**, *20*, 2609–2615.
37. Zhai, T. Y.; Ye, M. F.; Li, L.; Fang, X. S.; Liao, M. Y.; Li, Y. F.; Koide, Y. S.; Bando, Y.; Golberg, D. Single-Crystalline Sb2Se3 Nanowires for High-Performance Field Emitters and Photodetectors. *Adv. Mater.* **2010**, *22*, 4530–4533.
38. Fowler, R. H.; Nordheim, L. Electron Emission in Intense Electric Fields. *Proc. R. Soc. London, Ser. A* **1928**, *119*, 173–181.
39. Kim, G.; Jeong, B. W.; Ihm, J. Deep Levels in the Band Gap of the Carbon Nanotube with Vacancy-Related Defects. *Appl. Phys. Lett.* **2006**, *88*, 193107.
40. Kumar, M.; Okazaki, T.; Hiramatsu, M.; Ando, Y. The Use of Camphor-Grown Carbon Nanotube Array as an Efficient Field Emitter. *Carbon* **2007**, *45*, 1899–1904.
41. Zeng, B. Q.; Xiong, G. Y.; Chen, S.; Wang, W. Z.; Wang, D. Z.; Ren, Z. F. Enhancement of Field Emission of Aligned Carbon Nanotubes by Thermal Oxidation. *Appl. Phys. Lett.* **2006**, *89*, 223119.
42. Jeong, H. J.; Choi, H. K.; Kim, G. Y.; Song, Y. I.; Tong, Y.; Lim, S. C.; Lee, Y. H. Fabrication of Efficient Field Emitters with Thin Multiwalled Carbon Nanotubes Using Spray Method. *Carbon* **2006**, *44*, 2689–2693.
43. Dean, K. A.; Burgin, T. P.; Chalamala, B. R. Evaporation of Carbon Nanotubes During Electron Field Emission. *Appl. Phys. Lett.* **2001**, *79*, 1873–1875.